

**Spectra of mechanical cavity modes in distributed Bragg reflector based vertical GaAs resonators**S. Anguiano,<sup>1</sup> G. Rozas,<sup>1</sup> A. E. Bruchhausen,<sup>1</sup> A. Fainstein,<sup>1,\*</sup> B. Jusserand,<sup>2</sup> P. Senellart,<sup>3</sup> and A. Lemaître<sup>3</sup><sup>1</sup>*Centro Atómico Bariloche & Instituto Balseiro, C.N.E.A., 8400 San Carlos de Bariloche, Rio Negro, Argentina*<sup>2</sup>*Institut des NanoSciences de Paris, UMR 7588 C.N.R.S. - Université Pierre et Marie Curie, 75015 Paris, France*<sup>3</sup>*Laboratoire de Photonique et de Nanostructures, C.N.R.S., 91460 Marcoussis, France*

(Received 13 June 2014; revised manuscript received 16 July 2014; published 30 July 2014)

Distributed Bragg reflector based semiconductor resonators constitute paradigmatic systems where cavity optomechanical and optoelectronic phenomena can be simultaneously active in the same device. High GHz range mechanical frequencies and ultrastrong optomechanical couplings are additional attractive features for applications. We report here a detailed spectroscopic study of the fundamental optomechanical resonances of such a device. The existent challenge to study vibrational frequencies that are above the bandwidth of current electronics is solved using a purposely made tandem Fabry-Perot-triple spectrometer. A full theoretical description of the Raman process including electronic, vibrational, and optical confinement is presented to describe the experiments. These results open the path for the demonstration of polariton optomechanical phenomena in these devices.

DOI: [10.1103/PhysRevB.90.045314](https://doi.org/10.1103/PhysRevB.90.045314)

PACS number(s): 85.60.-q, 78.30.-j, 78.67.Pt

Distributed Bragg reflector (DBR) based microcavities combine the richness of novel optomechanical resonator phenomena [1–11], i.e., optomechanical nonlinearities, laser cooling [12–15], and phonon lasing [16,17], with the world of cavity optoelectronics, including controlled light emission and single-photon emitters [18], lasing [19,20], and polariton condensation [21].

For the GaAs/AlAs family of materials a resonator structure based on distributed Bragg reflectors (DBRs) and designed to confine photons (i.e., an optical microcavity) efficiently confines acoustic phonons of the same wavelength, strongly enhancing their interaction [22,23]. Indeed, a “magic coincidence” determines that the materials index of refraction, mass density, and sound speed, the physical quantities that determine the optical and acoustic device performance, are such that precisely the same structure designed to optimally confine light with the largest optical  $Q$  factor (that is, field amplification) will optimally confine the phonons with the largest attainable acoustic  $Q$  factor (that is, resonant displacement and strain). These structures constitute optomechanical devices that can attain very high mechanical and optical  $Q$  factors ( $Q \sim 10^5$ ), very low mechanical effective masses ( $m_{\text{eff}} \sim \text{pg}$ ), large optomechanical coupling factors ( $g_{\text{om}} \sim \text{THz/nm}$ ), and ultrahigh vibrational frequencies (sub-THz) [22]. Based on the demonstrated record optomechanical coupling it was predicted that stimulated emission of GHz phonons should occur in pillars of a few micrometers diameter under laser pump powers in the micro-milliwatt range. Quite interestingly, the studied planar microcavities based on DBRs can be designed so that, even with almost perfect mirrors, the phonon extraction out of the cavity is highly efficient.

One central feature to these unique DRB-based GaAs/AlAs optomechanical resonators is that precisely the same kind of structure is canonical to optoelectronic phenomena. In fact, the studied devices are based on the semiconductor vertical microcavity structures developed to demonstrate single-photon emitters, polariton condensates, and vertical

cavity surface emitting lasers (VCSELs). One could indeed envision a microcavity operating simultaneously as a VCSEL that could provide the required photons for stimulated emission of phonons under electronic injection [22]. Moreover, optomechanical resonators with embedded artificial atoms can be conceived, strongly coupling not only photons to vibrations, but also to excitons. Such “polariton optomechanical” resonators have been predicted to display novel phenomena, including unconventional [24] and ultrastrong optomechanical coupling (in the PHz/nm range) [25,26], and cooling at the single-polariton level [27]. We present here a detailed spectral study of the vibrations relevant to cavity optomechanical phenomena in these unique DBR-based hybrid optomechanical and optoelectronic resonators using a purposely made Fabry-Perot-triple spectrometer tandem. The results are analyzed using a full model for the Raman efficiency that accounts for the electronic, vibrational, and optical confinement existent in the structure.

The structure studied here is a  $\lambda/2$  bulk-GaAs planar microcavity enclosed by two distributed Bragg reflectors consisting of alternating  $\text{Ga}_{0.9}\text{Al}_{0.1}\text{As}/\text{Ga}_{0.05}\text{Al}_{0.95}\text{As}$   $\lambda/4$  layers, 28 pairs on the bottom, and 24 on top. The thickness of all layers was grown wedge shaped, so that the cavity mode could be tuned ( $\pm 50$  meV) around the room-temperature GaAs  $1s$  exciton transition  $\approx 1.42$  eV, by displacing the laser spot position. The optical  $Q$  factor is around  $1.4 \times 10^4$ . As previously demonstrated [22], such a structure displays confined mechanical modes in the  $\Omega \approx 20$  GHz range, with higher order modes at frequencies given by  $(2p + 1)\Omega$  ( $p$  being an integer).

To measure the mechanical modes, common cavity optomechanical experiments rely on the possibility to excite with a narrow-line continuous wave laser the resonator, and to detect with the appropriate resolution and sensitivity the generated vibrations. Optomechanical nonlinearities, cooling, and amplification emerge as outcomes of peculiar experiments based on these ingredients. To evidence these effects in the proposed domain of polariton optomechanics, vibrational spectra with frequencies in the 20–100 GHz range in cavities with  $Q$  factors in the  $10^4$ – $10^5$  range need to be generated,

\*afains@cab.cnea.gov.ar

manipulated, and monitored. Thus, concomitant with these novel technologies new challenges emerge: vibrational modes with these high frequencies lie above the limit of present electronics, but are too small to be studied with the best commercial dispersive spectrometers.

Typical cavity optomechanics spectroscopy exploits homodyne noise detection of narrow-line cw laser light scattered from the resonating structures. While this is the experiment of choice in the kHz-MHz range, fast detectors and ultrahigh bandwidth spectrum analyzers pose technological limits when GHz frequencies are aimed at. In the visible to near infrared wavelength range where polaritons are studied, homodyne detection experiments are difficult but still possible at 20 GHz. However this is certainly a technological limit, and a different approach is required for higher frequencies. In principle the same information would be accessible if the light scattered from the resonator were spectrally separated from the laser and analyzed (“noise” measurements result from the beating between the laser and spectrally shifted frequencies). This corresponds to the point of view of Brillouin or Raman scattering. Brillouin scattering using for example Sandercock interferometers is capable of discriminating excitations in the GHz range with high resolution. However, a problem arises if the studied spectra span frequency ranges larger than the free spectral range (FSR) of the interferometer. A compromise between resolution (small FSR) and covered spectra (large FSR) exists that, for the present study, leads to a no-win situation. High-resolution dispersive Raman spectrometers, on the other hand, can span the required spectral range, but do not have the required resolution. A triple-additive state-of-the-art Raman spectrometer has typically a resolution of  $\approx 0.3 \text{ cm}^{-1}$  ( $\approx 10 \text{ GHz}$ ) in the near infrared, so that features in this scale should be poorly resolved, if at all. Stray-light rejection in this energy range also becomes a major challenge. Briefly, the resolution of a Fabry-Perot interferometer is required, with in addition the spectral coverage, discrimination and stray light rejection of a high-resolution dispersive spectrometer. In order to study the optomechanical vibrations of the DBR-based resonator we have developed such a tandem setup, improving the resolution of the Raman spectrometer more than one order of magnitude. This allows at the same time the high-resolution measurement of vibrations down to  $\approx 0.01 \text{ cm}^{-1}$  (a few tenths of a GHz), with no upper limit [28].

The system is composed of a single-pass Fabry-Perot interferometer coupled to a T64000 Jobin-Yvon triple spectrometer operated in additive configuration. The light to be analyzed is collected from the sample by a lens, filtered through the FP, and then focused by a second lens into the entrance slit of the spectrometer. The FP contains two high-quality ( $\lambda/200$ ) dielectric mirrors for the near infrared (99% peak reflectivity centered at 870 nm), which are kept parallel at a fixed distance ( $0.5999 \pm 0.0001$ ) cm by three high-quality cylindrical silica spacers, leading to a  $\text{FSR} = (0.8335 \pm 0.0002) \text{ cm}^{-1}$  in vacuum. The mirrors are located in a sealed chamber connected to a gas distribution and vacuum system, which allows for the control of the pressure and composition of the gas inside it. The gas used was pure nitrogen. As the resolution of the spectrometer is better than the FSR of the FP but not enough to resolve the width of the transmission peaks, the acquired spectrum consists of several broad resolution-limited

peaks of which the relevant information is their integrated intensity. By repeating this procedure as a function of the gas pressure, we reconstruct the Raman profile [28]. The triple spectrometer is equipped with a liquid-N<sub>2</sub> cooled charge-coupled device (CCD) multichannel detector. The excitation is done using a near-infrared Ti:sapphire single-mode Spectra-Physics Matisse TS ring laser, the wavelength of which can be locked to an external confocal cavity with a precision better than  $2 \times 10^{-6} \text{ cm}^{-1}$ .

Cavity optomechanics spectroscopy was thus performed using such hybrid Fabry-Perot-triple spectrometer tandem in a double-resonant configuration in which both the laser *and* the scattered light are resonant with optical cavity modes of the structure. For the planar structure studied this can be accomplished by angle tuning and exploiting the in-plane dispersion of the optical cavity modes [29,30]. This is illustrated in Fig. 1, where the in-plane dispersion of photon modes of the resonator is shown, obtained from  $k$ -space imaging of light emitted from the device (residual gap photoluminescence). Here the color map is the measured photoluminescence intensity, while the dashed curve is calculated using standard matrix methods for light propagation in layered media. The dash-dotted horizontal and vertical lines and the arrows represent a typical experiment, by which a laser of wavelength  $\lambda_l$  (below the GaAs-cavity gap at  $\approx 872 \text{ nm}$ ) is coupled to the cavity at an angle  $\theta_0$ , and the scattered light at wavelength  $\lambda_s$  is resonantly collected along the normal to the device layers ( $\theta = 0$ ). The inset to the figure is a scheme of the experimental setup. By finely tuning the incidence angle  $\theta_0$  the frequency of specific vibrational features can be selectively amplified. Strong laser-light rejection (additional to that provided by the spectrometer) can be attained by filtering the collected light with a small aperture. In fact, the cavity structure helps for this purpose because light at the laser energy is emitted within a cone defined by the resonant angle  $\theta_0$ .

Figure 2 demonstrates how such angle tuning is performed. Raman spectra for different spot positions and using only the triple-additive configuration of the Raman spectrometer (no

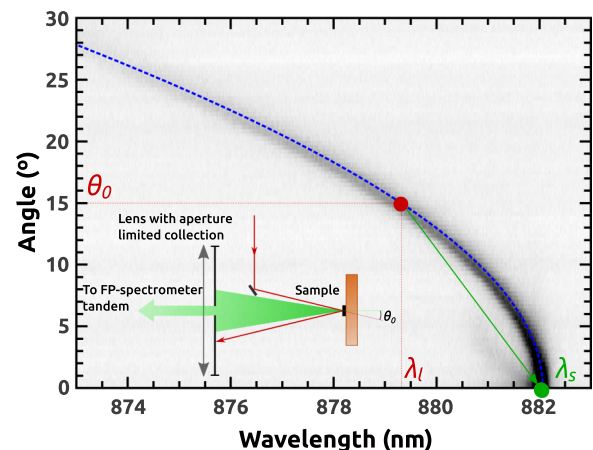


FIG. 1. (Color online) Color map corresponding to the in-plane dispersion of the optical cavity modes. The double-resonant Raman scattering process is accomplished by sending light at a specific angle  $\theta_0$  and wavelength  $\lambda_l$ , and collecting the  $\lambda_s$  scattered light at  $\theta = 0$ . The inset is a scheme of the experimental configuration.

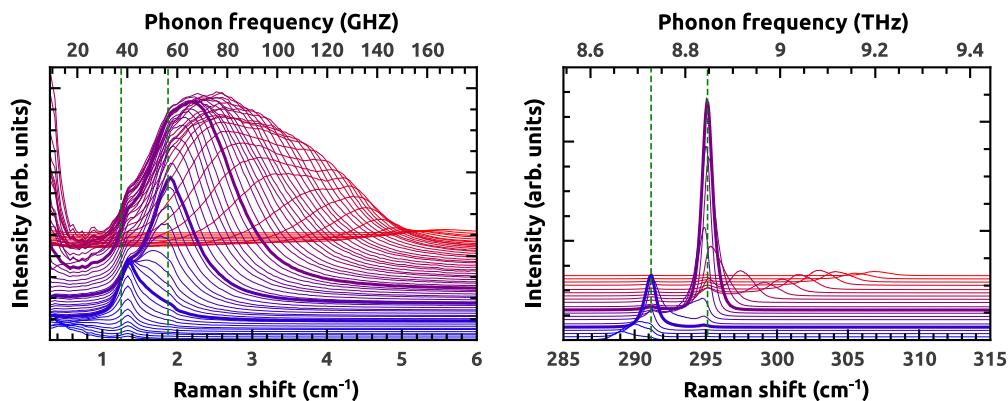


FIG. 2. (Color online) Raman spectra measured on different spots on the sample, so as to tune the optical cavity mode. Spectra were taken for double-resonant conditions with incidence angle  $\theta \approx 4^\circ$  (left) and  $\theta \approx 47^\circ$  (right), tuned to enhance the spectra corresponding to optomechanical vibrations and optical phonons of the structure, respectively. Vertical dashed lines and spectra with thicker curves are shown to highlight the peaks that can be identified as due to phonons.

Fabry-Perot interferometer included at this stage) are shown for two specific incidence angles:  $\theta \approx 47^\circ$  and  $\theta \approx 4^\circ$  for the selective double-resonant amplification of optical phonons and mechanical vibrations around  $\approx 295 \text{ cm}^{-1}$  and  $\approx 2.5 \text{ cm}^{-1}$ , respectively. In both cases the cavity mode can be observed redshifting in energy (increasing in Raman shift) from bottom to top for varying spot position, leading to the amplification of specific vibrational modes when the outgoing resonance condition is satisfied. The right panel corresponds to  $\theta \approx 47^\circ$ , and evidences optical phonons of the structure at  $\approx 291 \text{ cm}^{-1}$  and  $\approx 295 \text{ cm}^{-1}$  [31]. The left panel shows a detail of the low-energy vibrational spectra collected with  $\theta \approx 4^\circ$ . Here two broad features that could be assigned to Brillouin-Raman peaks can be identified at around  $1.3 \text{ cm}^{-1}$  and  $1.95 \text{ cm}^{-1}$ . We want to stress here that these spectra have been obtained with one of the highest-resolution pieces of Raman equipment available.

The spectra in Fig. 2 highlight the role of the optical cavity resonance, and the potential of the selective double-resonant configuration to amplify and detect specific vibrations at very different spectral ranges. At the same time it is quite clear that the vibrational spectra presumably assigned to optomechanical excitations of the structure are resolution limited. Figure 3 resumes the amount of information that is indeed contained in these spectra when the appropriate resolution is attained. To this purpose we show first in the top panel again spectra taken with the commercial triple-additive spectrometer now with a slightly smaller laser incidence angle ( $\theta \approx 3.4^\circ$ ) selected for double-resonant enhancement around  $1.9 \text{ cm}^{-1}$  (full darker curve). To help the identification of the observed features the calculated acoustic reflectivity (assuming a GaAs substrate on both sides of the structure) and phonon dispersion (for an infinite DBR) are displayed in the bottom panel. The stop bands associated with Brillouin zone-edge minigaps can be seen, and the cavity modes perfectly tuned to the center of these stop bands can be clearly identified. Comparison of the two panels demonstrates that the cavity modes are essentially invisible with this setup. Only a broad feature at the high-energy side of the Brillouin zone center modes at  $\approx 38 \text{ GHz}$  seems to contribute to the spectra.

That this is indeed the case is established only when the full potential of the Fabry-Perot spectrometer tandem is put

into play, as displayed in the middle panel of Fig. 3. The acquired spectra shown with a solid curve were obtained precisely in the same conditions as those in the top panel, with only the Fabry-Perot interferometer inserted in between the collection optics and the spectrometer, and by scanning the FP gas pressure to reconstruct the high-resolution Raman spectra as described above [28]. The richness of the spectra is striking: clear narrow cavity modes are observed precisely at

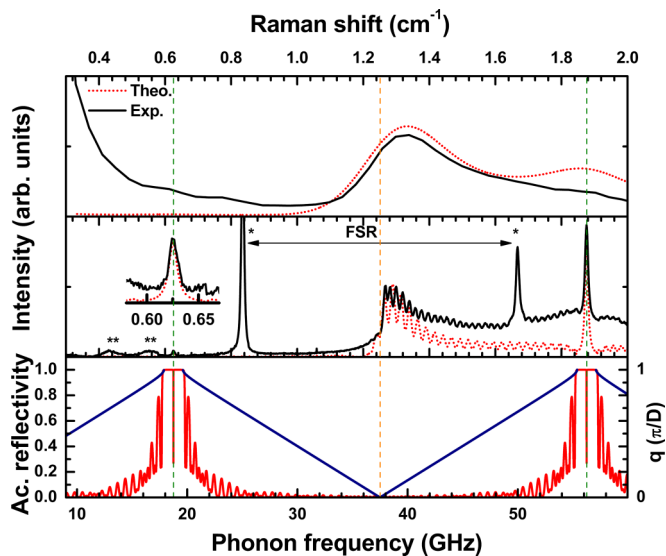


FIG. 3. (Color online) Raman spectra taken with incidence angle  $\theta \approx 3.4^\circ$  (double-resonant condition tuned around  $1.9 \text{ cm}^{-1}$ ) with the triple-additive spectrometer (top) and the Fabry-Perot-spectrometer tandem (middle). Solid darker curves correspond to the experiment, dotted curves to the model (see text for details). The peaks marked with single and double asterisks are assigned to laser light. In particular the strong peaks close to 25 and 50 GHz signal the successive tuning of the Fabry-Perot modes with the laser energy, their difference corresponding to the FSR. The bottom panel shows the calculated acoustic reflectivity of a microcavity surrounded by GaAs (instead of air in one side), and the acoustic dispersion of an infinite DBR. Vertical lines highlight relevant spectral features at the Brillouin zone edge and center.

the expected frequencies around 19 and 56 GHz, together with a broad contribution with fast oscillations at the high-energy edge of the Brillouin zone center modes around 38 GHz. It is only due to the ultrahigh resolution of the tandem that modes essential for the understanding of the optomechanics of these structures become visible. These modes are very narrow, their integrated oscillator force is comparatively weak, and thus their existence is mostly washed out even with an excellent state-of-the-art high-resolution commercial spectrometer.

The detailed understanding of the observed spectra is relevant for all cavity optomechanical measurement in these devices, irrespective of whether homodyne noise or Raman techniques are used. To this purpose we have performed extensive numerical simulations of the Raman spectra based on an implementation of the He-Sapriel model [32] to structures with arbitrary sequence of layers (dotted curves shown in Fig. 3). The model is a rigorous mathematical description of the scattering process, including the effects of electronic, phonon, and light confinement in the structure. Published data for the sound velocity and dielectric constants of the materials are used. Layer thicknesses are slightly varied around nominal values to fit the wavelength of the optical cavity mode at the specific sample position where the shown spectra were collected. The resonant character of the photoelastic coupling is taken into account by assuming a larger photoelastic coupling in GaAs (relative magnitude 10, 7, and 0 in GaAs, Ga<sub>0.9</sub>Al<sub>0.1</sub>As, and Al<sub>0.95</sub>Ga<sub>0.05</sub>As, respectively). The relative intensity of the 19 and 56 GHz modes is determined both by the spatial overlap of strain fields and electromagnetic mode, and by the scattering angle that defines the double-resonant condition. This latter value was selected to account for the experimental relative intensities obtained using the tandem setup. The calculated spectra are convoluted to account for the experimental resolution, with a Lorentzian of  $\sigma = 0.01 \text{ cm}^{-1}$  and a Gaussian of  $\sigma = 0.24 \text{ cm}^{-1}$  for the tandem and the additive Raman spectrometer, respectively. This means that the width of the measured cavity modes is resolution limited, so that it does not reflect the actual mode lifetime [33]. Because the experimental width is around  $\sigma = 0.01 \text{ cm}^{-1}$  (corresponding to an apparent lifetime of  $\approx 1 \text{ ns}$ ), this would imply a mechanical  $Q$  factor around 60 for the 19 GHz mode. The calculated  $Q$  factor, assuming that losses are only due to the escape towards the substrate, is however around  $3.7 \times 10^4$ . Roughness, inhomogeneous broadening, and anharmonicity existent in real samples may limit these values [33]. Unfortunately such studies are still out of reach of both reported techniques, either spectroscopic (as studied here) or time resolved (as in Ref. [22]).

The agreement between theory and experiment is remarkable, including the most subtle details. This demonstrates the strength of the model for the description of the optomechanical properties of the device. The spatial distribution of the relevant electromagnetic and vibrational modes are shown in Fig. 4. It becomes clear that the modes at 19 and 56 GHz correspond indeed to confined vibrations, while the broad feature around 38 GHz originates in modes that extend evenly through the whole structure. Note also that the 19 GHz is precisely the first-order breathing mode, the one at 56 GHz being its third harmonic.

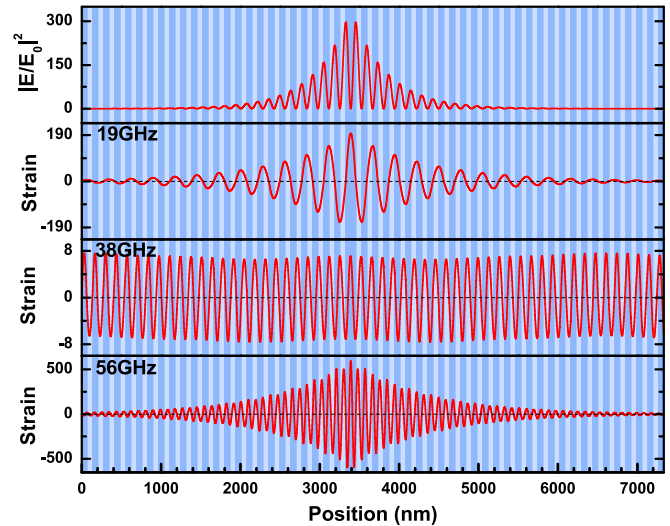


FIG. 4. (Color online) Calculated optical and acoustic modes of the optomechanical resonator. From top to bottom: electric intensity associated with the optical cavity mode, normalized to an incidence of amplitude 1, and strain associated with relevant modes at  $\approx 19$ , 38, and 56 GHz, appropriately normalized assuming the system in thermal equilibrium. Note the confined (extended) character of the modes at 19 and 56 (38) GHz.

The essential features of the model of Raman efficiency in a layered microcavity structure are captured by the simplified macroscopic expression of Raman scattering given by [34]

$$\sigma(\omega) \propto \frac{1}{\omega} [n(\omega) + 1] \left| \int_0^L dz [E_w(z)]^2 P(z) \frac{\partial u_w(z)}{\partial z} \right|^2, \quad (1)$$

with  $n(\omega)$  the Bose-Einstein statistical factor, and  $E_w(z)$  the amplitude of the electromagnetic field in the microcavity (a standing wave in the case of the optical cavity mode).  $P(z)$  is the photoelastic constant, defined by  $\Delta\epsilon(z) = P(z) \frac{\partial u_w(z)}{\partial z}$ , with  $\Delta\epsilon(z)$  the variation in the dielectric function induced by the oscillation displacement  $u_w(z)$ . The integral over space of strain and electromagnetic fields in Eq. (1) represents in bulk matter the wave-conservation relations (i.e., phase matching). For a forward scattering process this implies that the wave vector transferred from light to sound is zero. In a backscattering process (both coexist in a cavity) the transferred wave vector is  $q = 2k_L = 4\pi/\lambda$ , with  $q$  ( $k_L$ ) the phonon (light) wave vector, and  $\lambda$  the photon wavelength. Because of the cavity resonance thus  $q = 2k_L = 2\pi/D$ , with  $D$  the period of the DBR. In a reduced Brillouin zone scheme,  $2\pi/D = 0$ , implying that both forward- and backscattered waves lead to coupling of light only to  $q = 0$  (zone-center) phonons. Because the DBR is not infinite and includes a defect (the spacer), this wave-vector selection rule is somewhat relaxed, leading to the relatively broad peak at 38 GHz in Fig. 3. Modes are observed only at the high-energy side of the  $q = 0$  zone-center vibrations because of an additional parity selection rule. For a  $\lambda/2$  cavity with  $(\lambda/4, \lambda/4)$  DBR, optomechanical modes have predominant even (odd) strain distribution above (below) the first zone-center crossing within Ga<sub>0.9</sub>Al<sub>0.1</sub>As (where the photoelastic constant in the DBRs is nonzero). The coupling to the confined cavity modes can be better understood

in terms of the spatial overlap integral contained in Eq. (1). In fact, for such modes the spatial distribution of electric and strain fields overlaps precisely, and thus the selection rules end being essentially defined by parity. For the first and third harmonics of the cavity modes the strain is even, and thus (because the intensity of the electromagnetic field is also even) light coupling to these modes is allowed.

In conclusion, we have been able to observe and fully characterize the GHz-range spectra of mechanical vibrations of GaAs DBR-based resonators using a purposely developed hybrid dispersive/interferometric technique. The reported results open the path for the demonstration of strong-coupling and polariton optomechanics phenomena in these devices.

- 
- [1] O. Arcizet, P.-F. Cohadon, T. Briant, M. Pinard, and A. Heidmann, *Nature (London)* **444**, 71 (2006).
- [2] T. J. Kippenberg and K. J. Vahala, *Science* **321**, 1172 (2008).
- [3] J. D. Thompson, B. M. Zwickl, A. M. Jayich, F. Marquardt, S. M. Girvin, and J. G. E. Harris, *Nature (London)* **452**, 72 (2008).
- [4] M. Eichenfield, J. Chan, R. M. Camacho, K. J. Vahala, and O. Painter, *Nature (London)* **462**, 78 (2009).
- [5] M. S. Kang, A. Nazarkin, A. Brenn, and P. St. J. Russell, *Nat. Phys.* **5**, 276 (2009).
- [6] I. Favero and K. Karrai, *Nat. Photonics* **3**, 201 (2009).
- [7] F. Marquardt and S. M. Girvin, *Physics* **2**, 40 (2009).
- [8] S. Groeblacher, K. Hammerer, M. R. Vanner, and M. Aspelmeyer, *Nature (London)* **460**, 724 (2009).
- [9] A. Schliesser, O. Arcizet, R. Riviere, and T. J. Kippenberg, *Nat. Phys.* **5**, 509 (2009).
- [10] S. Weis, R. Rivière, S. Deléglise, E. Gavartin, O. Arcizet, A. Schliesser, and T. J. Kippenberg, *Science* **330**, 1520 (2010).
- [11] Q. Lin, J. Rosenberg, D. Chang, R. Camacho, M. Eichenfield, K. J. Vahala, and O. Painter, *Nat. Photonics* **4**, 236 (2010).
- [12] A. D. O'Connell *et al.*, *Nature (London)* **464**, 697 (2010).
- [13] J. D. Teufel *et al.*, *Nature (London)* **475**, 359 (2011).
- [14] J. Chan *et al.*, *Nature (London)* **478**, 89 (2011).
- [15] E. Verhagen, S. Deleglise, S. Weis, A. Schliesser, and T. J. Kippenberg, *Nature (London)* **482**, 63 (2012).
- [16] C. Zhao, L. Ju, H. Miao, S. Gras, Y. Fan, and D. G. Blair, *Phys. Rev. Lett.* **102**, 243902 (2009).
- [17] I. S. Grudinin, H. Lee, O. Painter, and K. J. Vahala, *Phys. Rev. Lett.* **104**, 083901 (2010).
- [18] A. Dousse, J. Suffczynski, A. Beveratos, O. Krebs, A. Lemaître, I. Sagnes, J. Bloch, P. Voisin, and P. Senellart, *Nature (London)* **466**, 217 (2010).
- [19] K. Iga, F. Koyama, and S. Kinoshita, *IEEE J. Quantum Electron.* **24**, 1845 (1988).
- [20] T. Someya, R. Werner, A. Forchel, M. Catalano, R. Cingolani, and Y. Arakawa, *Science* **285**, 1905 (1999).
- [21] E. Wertz, L. Ferrier, D. D. Solnyshkov, R. Johne, D. Sanvitto, A. Lemaître, I. Sagnes, R. Grousson, A. V. Kavokin, P. Senellart, G. Malpuech, and J. Bloch, *Nat. Phys.* **6**, 860 (2010).
- [22] A. Fainstein, N. D. Lanzillotti-Kimura, B. Jusserand, and B. Perrin, *Phys. Rev. Lett.* **110**, 037403 (2013).
- [23] For other proposals of nonlinear acousto-optic phenomena in devices that simultaneously confine photons and phonons in one-dimensional structures, see for example I. E. Psarobas, N. Papanikolaou, N. Stefanou, B. Djafari-Rouhani, B. Bonello, and V. Laude, *Phys. Rev. B* **82**, 174303 (2010) and references therein.
- [24] J. Restrepo, C. Ciuti, and I. Favero, *Phys. Rev. Lett.* **112**, 013601 (2014).
- [25] G. Rozas, A. Bruchhausen, A. Fainstein, B. Jusserand, and A. Lemaître (unpublished).
- [26] Yong-Chun Liu, Yun-Feng Xiao, You-Ling Chen, Xiao-Chong Yu, and Qihuang Gong, *Phys. Rev. Lett.* **111**, 083601 (2013).
- [27] O. Kyriienko, T. C. H. Liew, and I. A. Shelykh, *Phys. Rev. Lett.* **112**, 076402 (2014).
- [28] G. Rozas, B. Jusserand, and A. Fainstein, *Rev. Sci. Instrum.* **85**, 013103 (2014).
- [29] A. Fainstein, B. Jusserand, and V. Thierry-Mieg, *Phys. Rev. Lett.* **75**, 3764 (1995).
- [30] A. Fainstein and B. Jusserand, *Phys. Rev. B* **57**, 2402 (1998).
- [31] See A. Fainstein and B. Jusserand, *Phys. Rev. B* **54**, 11505 (1996) for a detailed discussion of optical phonons in layered microcavity structures.
- [32] Jianjun He, Bahram Djafari-Rouhani, and Jacques Sapriel, *Phys. Rev. B* **37**, 4086 (1988).
- [33] G. Rozas, M. F. Pascual Winter, B. Jusserand, A. Fainstein, B. Perrin, E. Semenova, and A. Lemaître, *Phys. Rev. Lett.* **102**, 015502 (2009).
- [34] A. Fainstein and B. Jusserand, in *Light Scattering in Solids IX*, edited by M. Cardona and R. Merlin (Springer, Heidelberg, 2007).